Astron. Astrophys. 343, 33–40 (1999)

ASTRONOMY AND ASTROPHYSICS

Reprocessing and variable cold absorption in the broad-line radio galaxy 3C 390.3

P. Grandi[1], **M. Guainazzi**[2], **F. Haardt**[3], **L. Maraschi**[4], **E. Massaro**[5], **G. Matt**[6], **L. Piro**[1], **and C.M. Urry**[7]

[1] Istituto di Astrofisica Spaziale, C.N.R., Area Ricerca di Roma Tor Vergata, I-00133 Roma, Italy
[2] Astrophysics Division, Space Science Department of ESA, ESTEC, Postbus 299, 2200 AG Noordwijk, The Netherlands
[3] Dipartimento di Fisica, Università di Milano, Via Celoria, I-20133 Milano, Italy
[4] Osservatorio Astronomico di Brera, Via Brera 28, I-20121 Milano, Italy
[5] Istituto Astronomico, Universita' di Roma, Unita' GIFCO-CNR Roma I, Via Lancisi 29, Roma, Italy
[6] Dipartimento di Fisica "E.Amaldi", Università degli Studi "Roma 3", Via della Vasca Navale 84, I-00146 Roma, Italy
[7] Space Telescope Science Institute, 3700 San Martin Drive, Baltimore, MD 21218, USA

Received 14 May 1998 / Accepted 26 October 1998

Abstract. A *BeppoSAX* observation of the Broad Line Radio–Galaxy 3C 390.3 is reported. For the first time, both the K_α iron line and a strong reflection hump, produced by the illumination of the primary X–ray emission on cold matter, are detected in this source. The 0.1–100 keV continuum is modeled by an absorbed hard power law ($\Gamma \sim 1.8$) reflected at high energies by material with a fairly large covering factor ($\Omega/2\pi \simeq 1$). The iron line is centered at $\simeq 6.4$ keV (rest frame), is intrinsically narrow ($\sigma = 73^{+207}_{-73}$ eV), and has an equivalent width of $\simeq 140$ eV.

We discuss the results in the context of current models for AGNs and suggest that the primary X–ray power law continuum is probably produced by a hot inner flow, while the reprocessed radiation comes from an outer cold thin disk, and/or from a thick torus at even larger radii. Further observations with *BeppoSAX* could distinguish between the latter two cases. Beamed radiation associated to the radio jet is unlikely to contribute significantly to the X–ray emission.

Finally, an historical study of the column density N_H, also reported here, shows that the absorption along the line of sight changes in time. The N_H time variability, which is not correlated with that of the primary continuum, seems to imply variations of the geometry of the absorber rather than variations in the ionization state of the gas.

Key words: galaxies: active – galaxies: individual: 3C 390.3 – radio continuum: galaxies – X-rays: galaxies

1. Introduction

In recent years, statistical studies of complete samples of extragalactic radio sources have suggested a unified scheme for radio–loud AGN. According to this picture, radio galaxies, radio–loud quasars, and blazars are the same physical objects seen at decreasing angles with respect to the jet axis (Antonucci 1993; Urry & Padovani, 1995). A similar scenario has been proposed for radio–quiet AGN (i.e., Seyfert 1 and Seyfert 2 galaxies; Antonucci & Miller 1985; Miller & Goodrich 1990). The common motivation for such unified schemes is that the radiation field is almost certainly *anisotropic*, which automatically implies orientation–dependent observational properties. Some degree of anisotropy could be caused by an opaque circumnuclear torus, which for some lines of sight may prevent direct view of the active nucleus and of the broad emission line region. In radio–loud AGN, additional anisotropy is likely due to relativistic beaming of the continuum produced in the jet.

Broadly speaking, a radio–loud source should show a featureless (or almost featureless) spectrum when observed face–on, a Seyfert 1–like spectrum at intermediate angles and a Seyfert 2–like spectrum when seen edge–on. Broad line Radio Galaxies (BLRG) and Narrow Line Radio Galaxies (NLRG) are therefore considered the radio–loud counterpart of Seyfert 1 and Seyfert 2 galaxies, respectively. However, it is still unclear whether the accretion processes are the same in radio–loud AGN and in Seyfert galaxies. Indeed, Rees et al. (1982) suggested that in radio galaxies the accreting gas flow is not in a cold, geometrically thin, disk configuration, but it rather forms a hot, geometrically thick, ion–supported torus, characterized by low radiative efficiency. The Advection Dominated Accretion Flow (ADAF) models, more recently proposed by other authors (see Narayan, Mahadevan & Quataert 1998, hereinafter NMQ, for a recent review), follow similar lines of thought. Shapiro, Lightman & Eardley (SLE, 1976) found a solution to the accretion problem that, in many respects, resembles the later ion–supported torus, and suggested its relevance for the black hole candidate Cygnus X–1. In the SLE solution, however, the energy produced in the flow by viscosity is locally radiated and advection is implicitly assumed to be negligible. A hot ion torus, surrounded by a geometrically thin cold accretion disk irradiated by the hard radiation produced by the torus, was proposed by Chen and Halpern (1989) in the context of BLRG showing double peaked emission lines, notably Arp 102B and 3C 390.3.

Send offprint requests to: P. Grandi

From the observational point of view the situation is still confused. *Ginga* data of radio–loud objects showed uncertain detection of the iron line and/or the reflection component (Nandra & Pounds 1994). *ASCA* observations at better energy resolution showed the presence of the iron line in several radio–loud AGNs, but did not constrain the reflection hump (Eracleous et al. 1997, Allen & Fabian 1992, Grandi et al. 1997a, Yamashita & Inoue 1996). It is then unclear whether a Seyfert–like nucleus is present in radio galaxies. The wide energy band ($\sim 0.1 - -100$ keV) covered by the instruments on board *BeppoSAX* is particularly appropriate to address the problem. For this reason, a *BeppoSAX* Core Program has been dedicated to the spectral study of bright radio galaxies ($F_{2-10\,keV} > 10^{-11}$ erg cm^{-2} sec^{-1}). Here we present the observation of 3C 390.3, the first source observed.

3C 390.3 is a well known Broad–Line Radio Galaxy (z=0.057) with an FRII morphology and a core showing superluminal motion (Alef et al. 1996). Its spectrum is characterized by double–peaked emission lines in the optical and UV bands (Eracleous and Halpern 1994, Zheng 1996, Wamsteker et al. 1997). The UV bump, typically observed in most Seyfert galaxies, is weak or even absent (Wamstecker et al. 1997). The Einstein–IPC data revealed the presence of a strong intrinsic absorption (Kruper et al. 1990). Ghosh and Soundararajaperumal (1991) claimed the presence of a soft excess in the EXOSAT data, but their results have not been confirmed by the later ROSAT and *ASCA* observations (Walter et al. 1994, Leighly et al. 1997). At higher energies, analysis of *Ginga* data produced ambiguous results. Inda et al. (1994) resolved the iron line at 6.4 keV but not the reflection component. Nandra & Pounds (1994) could give only an upper limit on the equivalent width of the emission line, but revealed a weak reflection component of small covering factor ($\Omega/2\pi \sim 0.4$). *ASCA* confirmed the presence of the iron K emission line (Eracleous et al. 1996, Leighly et al. 1997), but could not constrain the reflection hump, most probably because of the limited energy range. 3C 390.3 has also been detected by OSSE in the soft $\gamma-$ray domain, above 50 keV (Dermer & Gehrels 1995).

2. Data reduction

3C 390.3 was observed on Jan. 9–10, 1997, with the Narrow Field Instruments (NFI) of the *BeppoSAX* satellite (Parmar et al. 1997, Boella et al. 1997, Manzo et al. 1997 and Frontera et al. 1997). The data reduction followed the standard procedure. LECS and MECS cleaned photon lists and PDS background–subtracted products (spectrum and light curve) were obtained using `SAXDAS 1.3.0`, included in the `Ftools` package.

The LECS and the MECS (3 units) spectra were accumulated over circular regions of 4′ radius and the background spectra were extracted from blank field observations, using extraction regions on the detector equal to those of the source. The observed background–subtracted count rates are 0.18 ± 0.03, 0.37 ± 0.02 and 0.49 ± 0.032 with a net exposure time of 35 ksec, 100 ksec and 46 Ksec in the LECS (0.12–10 keV), MECS (1.5–10 keV) and PDS (13–100 keV), respectively.

The grouping files available at the *BeppoSAX* Scientific Data Center (http://www.sdc.asi.it/software/) were used to re–bin the data with the ftool GRPPHA. The data were rebinned so as to allow the use of the χ^2 statistic and, at the same time, to sample the spectral resolution of the instruments ($\Delta E/E = 8 \times (E/6)^{-0.5} FWHM\%$ for the LECS and the MECS; $\Delta E/E = 0.15 \times (E/60)^{-0.5} FWHM\%$ for the PDS). Publicly available matrices (September 1997 release) were used for all the instruments.

The LECS, MECS and PDS light curves were inspected to search for possible time variability, using the `XRONOS` package. A standard χ^2 test was applied to the average count rate in each light curve. We could not detect any flux variation in the whole 0.1–100 keV range during our observation. The χ^2 probability that the source was not constant is smaller than 10^{-3} in each instrument, independently of the temporal bin size used. This result confirms observations done with older X–ray missions, which never detected short time variability on time scales $\lesssim 1$ day (Shafer, Ward & Barr 1985; Ghosh & Soundararajaperumal 1991; Inda et al. 1994; Leighly et al. 1997).

3. Spectral analysis

The 3C 390.3 data were initially divided by the 3C 273 data collected during the *BeppoSAX* Science Verification Phase (SVP). This method allows a quick qualitative look at the spectrum without the need for complex models. The SVP spectrum of 3C 273 was chosen because it is well represented by a simple power law in the 1.5–200 keV. Only a very small deviation occurs at ~ 5.4 keV (observer frame) due to the presence of a weak iron line (EW~ 30 eV). The LECS data were not considered because of the spectral complexity of 3C 273 below 1 keV (Grandi et al. 1997b). The spectral ratio immediately evidenced the presence of a line at ~ 6.0 keV (as expected from neutral iron, taking into account the redshift of the source), and a clear excess above 10 keV.

Because of the complexity of the 3C 390.3 spectrum, we decided to perform the spectral analysis in two steps, studying the continuum and the emission line separately. Special care was also taken in determining the absorbing column density along the line of sight.

3.1. Continuum: primary emission and reflection component

We fitted the *BeppoSAX* data in XSPEC between 0.12 and 100 keV excluding the points in the energy interval 5.5–7.0 keV, where the emission line contributes significantly, aiming for the best possible determination of the continuum. The relative flux normalization between the LECS and MECS was left free to vary, whereas a miscalibration of 15% between the MECS and the PDS was assumed as indicated by NFI intercalibration analysis based on observations of 3C 273 (Grandi et al. in preparation).

We first tested a single power law model (PL), with low energy absorption. The best fit parameters are reported in Table 1, with 90% confidence limits. This model is unacceptable as it

Table 1. Fits to *BeppoSAX* continuum[a] of 3C 390.3

	A[b]	$N_H(10^{20}\,cm^{-2})$	Γ	Γ^c_{hard}	E^d_{break}	R	χ^2 (d.o.f)
PL	$5.1^{+0.2}_{-0.1}$	10^{+2}_{-1}	1.68±0.02	–	–	0	245 (190)
BKP	5.4±0.2	12^{+1}_{-2}	$1.72^{+0.04}_{-0.03}$	1.49±0.07	6.7±1.4	0	220(188)
PL+REF	5.6±.3	13±2	1.80±0.05	–	–	$0.9^{+0.5}_{-0.3}$	207.6(189)
CPL +REF	$5.6^{+0.4}_{-0.3}$	13±2	$1.80^{+0.05}_{-0.04}$	–	$380^{+\infty}_{-257}$	$1.2^{+0.4}_{-0.3}$	204.5(188)

[a] Data in the 5.5–7 keV energy band are not included in the fits.
[b] Normalization factor at 1 keV ($\times\ 10^{-3}$ photons cm^{-2} sec^{-1} keV^{-1}).
[c] High–energy power law for model BKP.
[d] Power–law break in model BKP, e–folding cut–off energy in model CPL+REF.

gives a large value of χ^2, corresponding to a chance probability of about 0.004. A broken power law model (BKP) gives a better fit (see Table 1), but still not good enough in terms of the χ^2 statistic (chance probability of 0.054).

We therefore tested a more complex spectral model including, in addition to a power law, a reflection component (PEXRAV in XSPEC; see Magdziarz & Zdziarski 1995). The PEXRAV model assumes that a cold reflector is irradiated by a primary isotropic X–ray source. The input X–ray spectrum can be modeled by a simple power law or by a power–law with a high energy exponential cut–off. The general functional form for this model is:

$$N(E) = A * \left[E^{-\Gamma} * e^{-E/E_c} + R * f_{ref}(E, i, \Gamma, E_c)\right],$$

where A is a global normalization factor at 1 keV (photons cm^{-2} sec^{-1} keV^{-1}), Γ the photon index, and E_c the cutoff e–folding energy. Setting E_c=0, the exponential term is excluded from the fitting formula, and a simple power law is taken as primary continuum. The reflection component f_{ref} is computed assuming a plane parallel semi–infinite medium irradiated by a point–like or optically thin X–ray source, and is a function of the angle i between the line of sight and the normal to the slab. We fixed i to 26^o as deduced from the UV and optical emission line measures (Eracleous & Halpern 1994 and Wamsteker et al. 1997), and from the radio jet superluminal motion (Eracleous et al. 1996). Finally, R is an additional scaling factor introduced to take into account roughly the solid angle subtended by the cold reflecting material to the X–ray source located above it, when different from 2π. R=1 corresponds to the scale free geometry assumed in the computation of f_{ref}. In principle, a change of the subtended solid angle would imply a change in the angular distribution of impinging photons, which in turn would change not just the *normalization* of the reflected spectrum, but also its *shape*. However, such an effect is small in comparison to the quality of available data, and the geometry is usually assumed to be simply described by the parameter R = $\Omega/2\pi$.

The MECS and PDS data are better reproduced by the model including reflection than by the single (PL) or broken power law (BKP) models. We initially assumed a simple power law input spectrum (PL+REF). The reduced χ^2 decreases from 1.17 to the well acceptable value of 1.09 (chance probability of 0.17). The

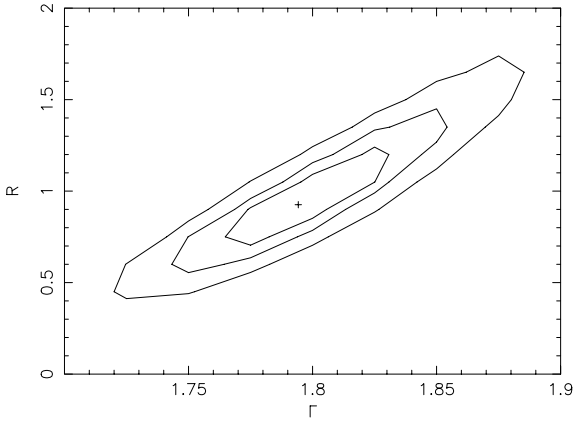

Fig. 1. Confidence contours for the photon index (Γ) and the amount of reflection (R) when the continuum is fitted with a power law reflected by cold matter (model PL+REF in Table 1).

reflection component is unambiguously detected at 99% confidence level, as evident from the contour plots shown in Fig. 1. We then included a high energy cutoff (CPL+REF), allowing E_c to vary. As expected, when the input X–ray spectrum is a power law with cut–off ($E_c \sim 400$ keV), the deduced value of R (R=1.2) is somewhat larger, but the increase is not statistically significant. In fact, in order to reproduce the observed Compton hump, the reflection component has to be a bit boosted to compensate for the reduction of primary photons at very high energies, which preferentially emerge, once down–scattered in the cold layers, around 20 keV. In any case, the improvement in χ^2 is not significant ($\Delta\chi^2 = 3$), and therefore the inclusion of a cut–off is not statistically required by the data. We note, however, that non–simultaneous *ASCA*, *Ginga*, and OSSE observations (Wozniak et al. 1998) suggest the presence of a break in the high energy spectrum of 3C 390.3. Also, the spectral index variations measured by *ASCA* (Leighly et al. 1997) indicate a pivot point at ~ 400 keV.

In any case, the amount of reflection required by the *BeppoSAX* data is larger than that previously measured by *Ginga* (R$\sim$ 0.3–0.4, (Nandra & Pounds 1994, Wozniak et al. 1998), possibly suggesting variations of the relative strength of the reflection hump with respect to the primary continuum.

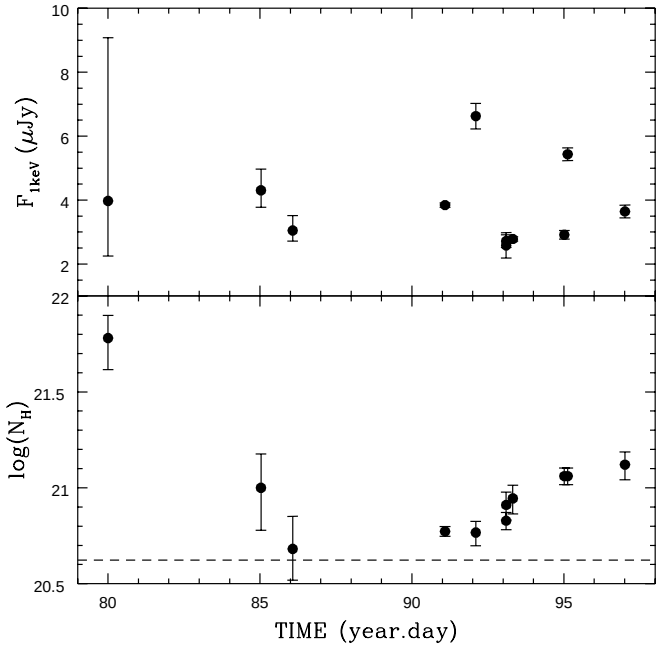

Fig. 2. (*upper panel*) Historical X–ray light curve of 3C 390.3. (*lower panel*) The column density is plotted as a function of time. The N_H trend was decreasing before 1987 and increasing after 1991. The dashed line corresponds to the Galactic column density

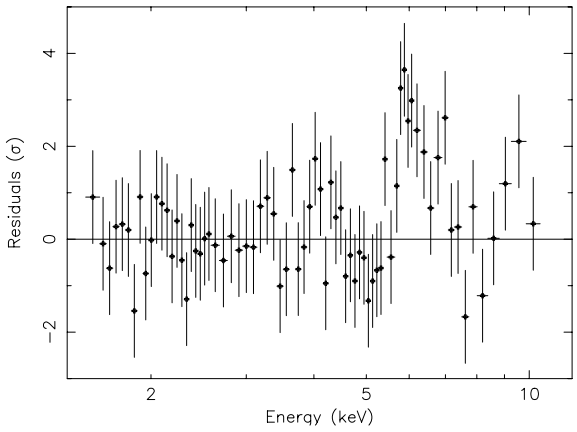

Fig. 3. MECS residuals (σ) to the data, when the continuum of emission is fitted with a power law reflected by cold material. The error bar corresponds to one sigma

Table 2. Best–fit parameters when a simple absorber power–law model is applied to the Feb. 3, 1985, and Mar 17–18, 1986, EXOSAT observations of 3C 390.3

Year	Instrument	N_H (10^{20} cm^{-2})	Γ	χ^2 (d.o.f.)
1985	ME+ AL + 3LEX	10^{+5}_{-3}	1.61 ± 0.10	50(43)
1986	ME+ AL + 3LEX	$4.6^{+2.6}_{-1.5}$	$1.56^{+0.10}_{-0.08}$	25(23)

3.2. Column density

The low energy absorption requires a column density larger than the Galactic value, $N_H^{Gal} = 4.2 \times 10^{20}$ cm^{-2} (Stark et al. 1992), for every model of the continuum we tested. Comparing our results with ROSAT data (Wamsteker et al. 1997), we noted that our determination of the column density is slightly larger. We then collected all the available information from the literature in order to investigate possible temporal variations of N_H. We re–analyzed two old EXOSAT observations performed in 1985 Feb. 3 and 1996 Mar. 17–18, respectively, as they provide a quasi–simultaneous coverage of the 0.01–10 keV band, and have a good signal–to–noise in the ME spectra (quality flag ≥ 3). The ME (1.8–10.0 keV) and LE (0.01–2 keV) data were simultaneously fitted with a simple power law with cold photoelectric absorption, which turned out to provide an adequate fit to the data in both the observations. The best fit values are reported in Table 2. No soft X–ray excess is required by the EXOSAT data. The LE data points lie on the extrapolation of the power–law continuum, which is basically determined by the ME statistics. This result is in disagreement with Ghosh and Soundararajaperumal (1991), who claimed that a soft excess is present in this source.

When the historical column density is plotted as a function of the date of observation, several interesting variations are evident, clearly indicating that temporal modifications of the cold material along the line of sight occurred, with an estimated time scale of a few years (see Fig. 2). In particular, the value of N_H seems to be steadily increasing since 1992, but was always found much lower than the first Einstein detection (Kruper et al. 1990).

We did not find any correlation between N_H and the intensity at 1 keV (see Fig. 2 and Table 3). This fact suggests that changes in the geometry of the absorber, rather than variations of its ionization state (as expected in the case of a warm absorber responding to an ionizing continuum), are probably responsible for the observed long term variability of N_H. Similar long–term absorption variability has been also observed in NGC4151 (Yaqoob et al. 1993).

3.3. Emission line

An excess in emission with respect to the power law plus reflection continuum is clearly present in the 5.5–7.0 keV energy interval (see Fig. 3). The statistical significance of this excess, estimated by the quadratic sum of the deviations in each bin, is at the level of $\simeq 7\sigma$. The excess is most likely produced by an Fe fluorescent line, for which we could estimate, using a gaussian profile, a flux of 3.63 (-1.45,+0.78) $\times 10^{-5}$ ph cm^{-2} sec^{-1} (at the 90% confidence level for one interesting parameter), corresponding to an equivalent width of 136 (-36,+40) eV. The line centroid lies at 6.39 (-0.09,+0.10) keV (rest frame), compatible with Kα line emission from neutral iron located at the source redshift. The line is not resolved: the intrinsic width can be estimated from the fits as 73 (-73,+207) eV, indicative of a narrow feature. The line flux and the intrinsic width confidence contours are shown in Fig. 4. These line best fit values are consistent with those of previous *ASCA* observations (Eracleous et al. 1996, Leighly et al. 1997): in fact the line intensity derived

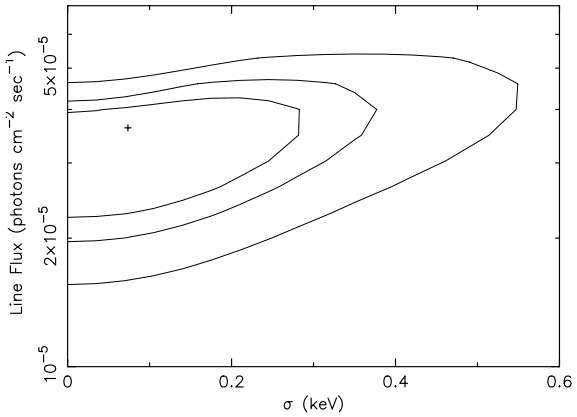

Fig. 4. Confidence contours for the line flux and the intrinsic width when the feature is fitted with a gaussian profile.

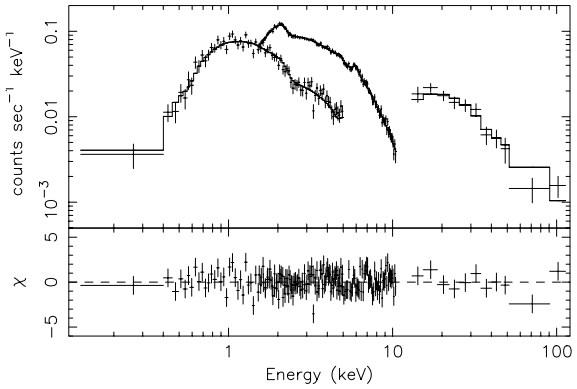

Fig. 5. Photon spectrum (*upper panel*) and residuals (*lower panel*) when a power law plus reflection and a gaussian line are fitted to 0.12–100 keV *BeppoSAX* data

from either *Ginga*, *ASCA* or *BeppoSAX* is consistent with being constant within the rather large errors (cf. Wozniak et al. 1998).

In Fig. 5 the total 0.1–100 keV photon spectrum is shown with the residuals to a power–law–plus–reflection model when the gaussian line is added to the fit.

4. Discussion

The detection of the iron line and of the reflection component in the *BeppoSAX* observation of 3C 390.3 indicates that beamed non–thermal radiation does not contribute significantly to the X–ray continuum. This is probably true independently of the brightness of the X–ray source, because a strong iron line ($EW \sim 130$) was also detected by *ASCA* in 1995 when the source flux was about 1.5 times larger than the *BeppoSAX* value (Leighly et al. 1997).

In 1995, 3C 390.3 was the object of a multifrequency campaign which included IUE, ROSAT and *ASCA* observations (Leighly et al. 1997, O'Brien et al. 1998). The UV and X–ray light curves, covering a period of about 8 months with a regular 3 day sampling, showed similar forms and variability amplitudes. As pointed out by O'Brien & Leighly (1997), if the UV were a direct extension of the X–ray emission, the two

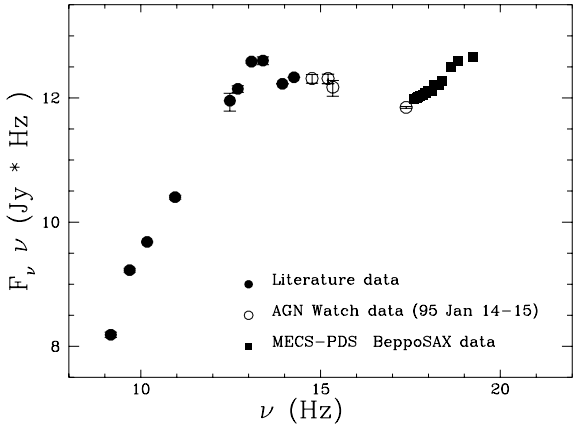

Fig. 6. Spectral energy distribution of 3C 390.3, from non-simultaneous observations. Radio-mm-infrared data (filled circles) are taken from literature (see text). Simultaneous optical UV and X-ray data (open circles) refer to the observation on 1995 January 14–15. The MECS and PDS data (filled squares) have been rebinned.

light curves should show different variability amplitudes, because the *ASCA* spectral slopes from two observations during the monitoring differed by $\Delta\alpha = 0.1$.

It is therefore likely that (at least part of) the UV is due to reprocessing of X–rays. Indeed, an excess of UV emission above the X–ray power law extrapolation (the blue bump) was noted by Walter et al. (1994) using simultaneous ROSAT–IUE observations performed during the ROSAT all–sky survey. However, the blue bump component, if present, is weak, as also indicated by the historical compilation of non–simultaneous ultraviolet and X–ray data of Wamsteker et al. (1997). The lack of a soft X–ray excess attested by several satellites (Walter et al. 1994, Eracleous et al. 1996, Leighly et al. 1997) and confirmed by our data (and by the re–analysis of the EXOSAT observations) further strengthens this conclusion.

In Fig. 6 the radio to γ–ray energy distribution of the 3C 390.3 is shown. Data from the literature (Rudnick et al. 1986, Steppe et al. 1988, Knapp et al. 1990, Poggioli 1991) are combined with the simultaneous optical–UV–X-ray data collected on 1995 January 14–15 during a 3C 390.3 multifrequency campaign (Leighly et al. 1997, Dietrich et al. 1998, O'Brien et al. 1988). The radio points correspond to the core flux only. Optical and UV measurements collected on 1995 January 14–15 refer to the continuum emission dereddened with the extinction curve of Seaton (1979) assuming Av=0.708. The visual extinction was deduced by the N_H column density measured by a simultaneous *ASCA* observation performed on 1995 January 15 (Leighly et al. 1997). On that occasion 3C 390.3 was in a state of brightness very similar to that observed by *BeppoSAX* later, as can be seen in Fig. 6, where the *ASCA* flux at 1 keV is plotted together with the MECS and PDS data. For the sake of clarity, the MECS and PDS data have been rebinned in order to have a signal to noise ratio of about 50 and 10 per each bin, respectively.

Fig. 6 shows that the energetics are dominated by the high energy end of the power–law, and by the large IR emission. The power emitted in the UV is definitely smaller than that in

Table 3. Absorbing column density history

Satellite/Instrument	Date of obs. Year.day	$N_H(cm^{-2})$ $(\times 10^{20})$	$Flux_{1\ keV}$ μJy	References
EINSTEIN/IPC	80.001	60 ± 19	$4.0^{+5.1}_{-1.7}$	Kruper et al. 1990
EXOSAT/LE+ME	85.033	10^{+5}_{-3}	$4.3^{+0.7}_{-0.5}$	this paper
EXOSAT/LE+ME	86.076	$4.6^{+2.6}_{-1.5}$	$3.1^{+0.5}_{-0.3}$	this paper
ROSAT/PSPC	91.089	5.9 ± 0.4	3.8 ± 0.1	Wamsteker et al. (1997)
ROSAT/PSPC	92.101	$5.8^{+0.8}_{-0.7}$	6.6 ± 0.4	this paper
ROSAT/PSPC	93.101	6.7 ± 0.7	2.6 ± 0.4	Wamsteker et al. (1997)
ROSAT/PSPC	93.102	8.1 ± 1.4	2.7 ± 0.2	Wamsteker et al. (1997)
ASCA/SIS	93.320	8.8 ± 1.5	2.8 ± 0.1	Eracleous et al. (1996)
ASCA/SIS	95.015	11 ± 1	2.9 ± 0.1	Leighly et al. (1997)
ASCA/SIS	95.125	11 ± 1	5.4 ± 0.2	Leighly et al. (1997)
BeppoSAX/LE+ME+PDS	97.009	13 ± 2	3.6 ± 0.2	this paper

the X-ray to hard X-ray component. This is consistent with the results of Woźniak et al. (1998), which show that during spectral variations the total energy output in X–rays does not change (see their Fig. 5).

All these facts indicate that the UV–emitting, optically thick gas must subtend a relatively small solid angle to the X–ray source, otherwise strong reprocessing would give rise to a thermal UV component that is energetically important and efficient cooling would steepen the X–ray power–law. On the other hand, as discussed in Sect. 3, the observed reflection hump and iron line need a fairly large covering factor of reprocessing material in order to be accounted for. How can these two, apparently contradictory, constraints be matched?

There are basically two models under discussion to account for X-ray emission from accretion disks in AGN:

1. A Seyfert–like model that assumes a geometrically thin accretion disk (Shakura & Sunyaev 1973), which is responsible for the UV thermal emission and for the reprocessing of (part of) the X–ray photons. The high energy photons are produced by an active corona embedding the inner portion of the cold accretion disk (Liang 1979, Haardt & Maraschi 1991, 1993). In this class of models, the Compton parameter is kept fixed by the energetic feedback linking the disk and the corona. UV photons in the disk are produced by thermalization of the absorbed X–rays, and X–rays in the corona are produced by inverse Comptonization of the UV disk radiation;
2. A hot accretion flow model, such as the original two–temperature solution introduced by SLE or the ion–supported torus proposed by Ichimaru (1977), and Rees et al. (1982), or its modern version, the ADAF (see NMQ for a review and all the relevant references). In the ion–supported torus and in the ADAF, relevant for low to modest accretion rates, the small gas density makes Coulomb collisions very ineffective in transferring energy from the ions (which are supposed to be directly energized by viscous stresses) to the electrons which bear the ultimate responsibility of radiating away the heat and cooling the gas. The direct consequence is the formation of a hot, two–temperature plasma in the inner region of the flow. In contrast, in the SLE solution the energy deposited in the gas is assumed to be locally radiated. In both classes of models, at larger distances from the black hole, the flow is thought to be described by a standard cooling–dominated thin disk (e.g., Mahadevan 1977).

From the point of view of the formation of the radiation spectrum, the main difference between the two pictures is the presence (in the disk–corona system) or the absence (in the ion–supported torus) of optically thick cold matter close to the X–ray source providing (or not) soft photons for the Comptonization mechanism. In the absence of a soft photon input from thermal optically thick gas, the seed photons are provided by cyclo-synchrotron radiation by the electrons themselves, yielding a power law which extends from the far IR up to hard X-rays with spectral index fixed by the accretion rate.

In the case of 3C 390.3, although a disk–corona model could explain the strong correlation between the IUE and X–ray light curves, the absence of a soft excess and the weakness of a possible blue bump argues against a large fraction of reprocessed radiation. An optically thick corona radiating all the available gravitational power could in principle scatter off all the black body photons from the accretion disk and hence produce a unique Compton–scattered power law (Haardt & Maraschi, 1993), with weak or absent signature of thermal emission. In this case, however, such a disk–corona system would give rise to a power law spectrum steeper than observed ($\Gamma \gtrsim 2$). In order to produce an X–ray power–law as flat as observed, one has to assume a photon–starved corona. Thus the required geometry is one in which the UV–emitting layer is at least partly external with respect to the region containing the hot electrons.

A completely hot inner flow, on the other hand, is a plausible description of the nuclear region. A hot inner region can in fact explain the lack of soft excess and the weak UV bump, which might still be the signature of an external standard cold thin disk. The ion–supported torus, or the ADAF, is one of the possible stable configurations of gas accreting onto a black hole. The optical to X–ray radiation is due to Compton cooling of the hot thermal electrons (with temperature $\sim 10^9$ K), scattering off soft free–free and cyclo–synchrotron photons. If the accretion

rate is high (but still below the ADAF critical accretion rate, $\dot{m}_{\rm crit} \simeq 0.1 \dot{m}_{\rm Edd}$, see NMQ), the bremsstrahlung contribution to the X–ray spectrum is negligible, and the X–ray continuum is hard ($\Gamma < 2$). In the case of 3C 390.3, the bolometric luminosity estimated from Fig. 6 is $L \sim 3 \times 10^{45}$ erg sec^{-1}. If we assume a central mass of $\sim$ 1–4 $\times 10^8$ M$_\odot$ (Wamsteker et al. 1997), the luminosity in Eddington units is $L/L_{Edd} \sim 0.05$–0.2., which would place 3C 390.3 in the range of high accretion rate ADAFs, consistent with the hard X–ray continuum. We note nevertheless that with this model the similarity of the spectral shape of 3C 390.3 to that of Seyfert galaxies would be coincidental.

If the accretion flow at larger radii is in the form of a standard thin disk, the weak blue bump could be also explained, as due to local energy release, and reprocessing of the (small) fraction of the X–rays intercepted and reprocessed by the cold matter. A flat infinite disk illuminated by a central hot ion–supported torus cannot intercept more than 25% of the primary continuum (Chen & Halpern 1989), adequate for the observed UV emission in this case, but not for the observed reflection component and for the iron line EW. It is then necessary that further cold material, encircling the central source, is shaped like a warped disk or a thick dusty torus at parsec distances. These geometries can ensure large covering factors, and produce a broad reflection hump practically indistinguishable (at this sensitivity level) from that arising from an infinite plane parallel medium (Ghisellini, Haardt & Matt, 1994; Krolik, Madau & Zycki, 1994). In particular, the K$_\alpha$ feature is expected to be narrow, in agreement with the iron line profiles observed by *BeppoSAX* ($\sigma = 70^{-70}_{+207}$ eV) and *ASCA* (Eracleous et al. 1997). The energetics would not be a problem in this picture, as most of the X–rays are absorbed at large distances from the source, and then re–emitted as IR radiation, rather than in the form of a UV bump as in the case of a Seyfert–like geometry. A simple test of this model would be the absence of short term variability both in the intensity of the Fe Line (Wozniak et al. 1998) and of the reflection component. For the latter, further *BeppoSAX* observations would be valuable.

An inner hot torus surrounded by an outer cold thin disk was already proposed by Chen and Halpern (1989) to explain the optical properties of BLRGs with double peaked emission lines and in particular of 3C 390.3. Our observations independently strengthen this picture. Whether this configuration can be consistent with the SLE solution, with the ion–supported torus, and/or with the ADAF accretion models is a matter of future investigations, beyond the scope of the present paper.

Finally, an important result of our studies is the discovery in 3C 390.3 of temporal variations of the local column density. The origin of the N$_{\rm H}$ variability is unknown. The presence of a warm absorber, usually invoked to explain modification of the column density in Seyfert galaxies, seems unlikely in 3C 390.3. The lack of features in absorption/emission in the soft X–ray spectrum and the absence of any correlation between the N$_{\rm H}$ values and the X–ray flux argue against this possibility. The long term variations can be better explained by geometrical modifications of a cold absorber.

5. Summary

We have presented *BeppoSAX* observation of the BLRG 3C 390.3. The X–ray data are well represented by an absorbed hard power law, plus a narrow K_α iron line and a Compton reflection component. No X-ray soft excess is required by the data in agreement with the results of previous X-ray satellites.

Considering also that a weak blue bump seems to characterize this source, we conclude that:

1. Beamed non–thermal X–ray continuum does not significantly contaminate the nuclear emission.
2. Material able to absorb and thermalize the X–rays is not present close to the X–ray source (otherwise we would observe a luminous UV to soft X–ray thermal component).
3. However, such material must lie at some distance and intercept a fraction $\sim$ 50% of the X–rays (otherwise we would not observe any reflection hump and iron line).

The model that better accounts for these results is a hot, X–ray emitting inner accretion flow. Roughly half of the X–ray radiation illuminates outer, cold, IR emitting material, possibly in the form of a warped disk and/or a dusty torus, producing the reflection hump and the narrow emission line. At this stage, it is premature to assess the nature of the hot inner flow. Different models (i.e., the ion–supported torus, the ADAF, or the SLE) could possibly be compared by studying UV–to–X–ray spectral variability on long time scales. For this aim, further broad–band observations are most welcome.

Finally we have presented a study of the time variations of N$_{\rm H}$, based on all the available historical data. We have shown, for the first time, that the column density in this source changes on time scale of years independent of variations in the X–ray flux. It is difficult to relate the variations of the absorber to changes of the ionization state of the medium along our line of sight. Geometrical modifications of the absorber would better account for the long term N$_{\rm H}$ variations.

Acknowledgements. We are grateful to G. Palumbo for critical reading of the manuscript. We would like to thank T. Yaqoob, W. Wamsteker for useful discussions, and L. Angelini for help in reducing the archival EXOSAT data. We wish to thank the referee for useful comments on the manuscript.

References

Alef W., Wu S.Y., Pruss E., Kellermann K.I., Qiu Y.H., 1996, A&A 308, 376
Allen S.W., Fabian A.C., 1992, MNRAS 258, 29p
Antonucci R.R.J., 1993, ARA&A 31, 473
Antonucci R.R.J., Miller J.S., 1985, ApJ 297, 621
Boella G., Chiappetti L., Conti G., et al., 1997, A&A 122, 327
Chen K., Halpern J.P., 1989, ApJ 344, 115
Cusuamano G., et al., 1998, A&A, in press
Dermer C.D., Gehrels N., 1995, ApJ 447, 103
Dietrich M. et al., 1998, ApJS 115, 185
Eracleous M., Halpern J.P., 1994, ApJS 90, 1
Eracleous M., Halpern J.P., Livio M., 1996, ApJ 459, 89
Frontera F., et al., 1997, A&AS 122, 357

Ghisellini G., Haardt F., Matt G., 1994, MNRAS 267, 743
Ghosh K.K., Soundararajaperumal S., 1991, AJ 102, 1298,ApJ 398, 157
Grandi P., Sambruna R.M., Maraschi L., et al., 1997a, ApJ 487, 636
Grandi P., et al., 1997b, A&A 325, L17
Haardt F., Maraschi L., 1991, ApJ 380, L51
Haardt F., Maraschi L., 1993, ApJ 413, 507
Ichimaru S., 1977, ApJ 840
Inda M., Makishima Y., Tashiro M., et al., 1994, ApJ 420, 143
Knapp G.R., Bies W.E., van Gorkom J.H., 1990, AJ 99, 476
Krolik J.H., Madau P., Zycki P.T., 1994, 420, L57
Kruper J.S., Urry C.M., Canizares C.R., 1991, ApJS 74, 347
Leighly K.M., O'Brien P.T., Edelson R., et al., 1997, ApJ 483, 767
Liang E.P.T, 1979, ApJ 231, L111
O'Brien P.T., Leighly K.M., 1997, A&AR 21, 67
O' Brien P. T., Dietrich M., Leighly K., et al., 1998, ApJS, in press
Magdziarz P., Zdziarski A.A., 1995, MNRAS 273, 837
Mahadevan R., 1997, ApJ 477, 585
Matt G., Perola G.C., Piro L., 1991, A&A 247, 25
Miller J.S., Goodrich R.W., 1990, ApJ 355, 456
Nandra K., Pounds K.A., 1994, MNRAS 268, 405
Narayan R., Mahadevan R., Quataert E., 1998, In: Abramowicz M.A., Bjornsson G., Pringle J.E. (eds.) The Theory of Black Hole Accretion Disk. in press (NMQ) (astro–ph/9803141)
Parmar A.N., Martin D.D.E., Bavdaz M., et al., 1997, A&AS 122, 309
Piran T., 1978, ApJ 221, 652
Poggioli M., 1991, Thesis, University of Bologna
Rees M.J., Begelman M.C., Blandford R.D., Phinney E.S., 1982, Nat 295, 17
Rudnick L., Jones T.W., Fiedler R., 1986, AJ 91, 1011
Seaton M.J., 1979, MNRAS 187, 73P
Shafer R., Ward M., Barr P., 1985, Space Sci. Rev. 40, 637
Shakura N.I., Sunyaev R.A., 1973, A&A 24, 337
Shapiro S.L., Lightman A.P., Eardley D.M., 1976, ApJ 204, 187
Stark, et al., 1992, ApJS, 78, 77
Steppe H., Saler C.J., Chini R., et al., 1988, A&AS 75, 317
Urry C.M., Padovani P., 1995, PASP 107,803
Walter R., Orr A., Courvoisier T.J.-L., et al., 1994 A&A 285, 119
Wamsteker W., Wang T., Norbert S., Vio R., 1997, MNRAS 288, 225
Williams O.R., Turner M.J.L., Stewart G.C., et al., 1992 ApJ 398, 157
Wozniak P.R., Zdziarski A.A., Smith D., et al., 1988, MNRAS 299, 449
Yamashita A., Inoue H., 1996, In: Makino F., Mitsuda K. (eds.) X–ray Imaging and Spectroscopy of Cosmic Hot Plasma. Universal Academy Press, Tokyo, Japan, p. 313
Yaqoob T., Warwick R.S., Makino F., et al., 1993, MNRAS 262, 435
Zheng W., 1996, AJ 111, 1498